





Particle Filter Based Multi-sensor Fusion for Remaining Service Life Estimation of Energized LV-Aerial Bundled Cables

Taimoor Zafar*1, Muhammad Hussain², Qamar Ud Din Memon², and Syed Zia Uddin¹ Electrical Engineering Department, Bahria University, Karachi, Pakistan

²Software Engineering Department, Bahria University, Karachi, Pakistan

*Correspondence: Taimoor Zafar and taimoorzafar.bukc@bahria.edu.pk

Citation | Zafar. T, Hussain. M, Memon. Q, Uddin, Zia. S "Particle Filter Based Multi-sensor Fusion for Remaining Service Life Estimation of Energized LV-Aerial Bundled Cables", IJIST,

Vol. 6 Issue. 2 pp 664-687, June 2024

DOI | https://doi.org/10.33411/ijist/202462664687

Received | May 20, 2024 **Revised** | June 03, 2024 **Accepted** | June 08, 2024 **Published** | June 12, 2024.

erial Bundled Cables (ABC) consist of several wires that contain numerous layers of thermal insulation, which reduces the risk of theft. Nonetheless, there have been regular reports of rapid degeneration of such cables in coastal areas, resulting in multiple unplanned breakdowns. This study employs the data, collected from field-based nondestructive assessment techniques such as ultrasonic listening and thermal imaging. There is a pressing need for advanced tools to estimate the remaining lifespan of ABCs deployed along coastlines. This paper presents a novel approach using a particle filter-based fusion of multiple sensors framework for estimating the Remaining Useful Life (RUL) of in-service ABCs in a severe coastal atmosphere. The use of multi-sensor measurement data improves the accuracy and reliability of the RUL estimation. This will allow electric power distribution companies to plan maintenance and replacement activities well in time. In the reported research work, the f-step prediction scheme under the framework of the Particle filter algorithm is implemented to predict the posterior density function of degradation growth in the cable insulation. The Particle Filter (PF) method performs effectively with nonlinear state transitions and measurement functions, even when addressing non-Gaussian or multidimensional noise variations. The technique also contains a step error calculation approach for determining forecast accuracy when measurement data is missing. The encouraging outcomes of this strategy illustrate its efficacy.

Keywords: Particle Filtering, Multisensory Fusion, Predictive Based Maintenance, Degradation Growth Rate, and Aerial Bundled Cables (ABCs).





























Introduction:

The overhead transmission lines, electric poles, and transformers are the essential parts of the electrical supply and power distribution network. The power supply shutdown often occurs due to the failures in power distribution lines. Normally, bare conductor cables and insulated conductor cables are used in the power distribution network [1], [2]. The insulated conductor cables are widely used due to their several advantages including safety and lesser chance of short-circuiting in the presence of high wind pressure [1], [2], [3]. Despite these advantages, monitoring the health of covered conductors in abrasive and harmful atmospheric conditions, especially in coastal regions, is challenging [4].

Three types of insulated conductor cables are reported in [5]; Covered Conductors (CCs), Spacer Cables (SCs), and Aerial Bundled Cables (ABCs). Among these only ABCs are multilayered bundled cables and their XLPE insulation makes them useful where chances of electricity pilferage through line tapping are high [6], [7]. ABCs have a longer service life in areas that are not shoreline, and their performance parameters are not known for coastal areas [2], [8], [9]. The authors in [10], [11], and [12], reported that the insulation of ABCs is degraded in the presence of high solar radiation and high moisture content under variable load conditions, leading to unexpected supply shutdowns which is an undesirable event for the good economic growth of any country. Therefore, regular health inspection and future health estimation of insulated power transmission lines are highly significant to ensure continuous power supply, especially in coastal regions.

Table 1: List of Notations

Notation	Description	Notation	Description
n	Discretized Location	E _{n,1}	One step error for n moments
x_n	Defects depths at a separate position (state)	$E_{n,2}$	Two-step error for n moments
$\mathbf{z}_{\mathbf{n}}$	NDE measurement at discretized location	f	The overall number necessary subsequent states ($f = 1, 2, 3,4,5,F$)
N	The overall number of discretized or independent locations	$\mathbf{u}_{\mathbf{n}}^{\mathbf{i}}$	The overall number of i^{th} stages with corresponding weights w_n^i for n instances at n instants.
0	Measurement mode	$w_n^{i,o}$	Assigned normalized weight to x_n^i by o^{th} measurement mode
0	Total number of measuring modes	NDT	Nondestructive Testing
$\overline{\mathbf{z}}_{\mathbf{n}}$	Measurements at separated locations as a result of O measuring modes	IPC	Insulation Piercing Connector
$\vec{\mathrm{Z}}$	The overall number of measurements corresponds with all measuring modes. O for all distinct places/positions N	ABCs	Aerial Bundled Cables
\vec{X}	Set of states	LV	Low Voltage
\mathbf{u}^*	State with updated weight	НТ	High voltage Transmission
û	State without updated weight	SIR	Sampling Importance Sampling



	Measurements at instant n data	EMD	Empirical Mode		
y_n	(with additive noise)	EMD	Decomposition		
$y_{1:n}$	Previous measurements 1 to n	PF	Particle Filter		
$p(u_n y_{1:n})$	Posterior density	RUL	Remaining Useful Life		
$p(y_n u_n)$	Likelihood density	UT	Ultrasonic Testing		
$p(u_n y_n - 1)$	Prior density	ННТ	Hilbert Huang Transform		
x_n^i	i th sample (particle) at n discrete location	ROI	Region of Interest		
$w_n^i \\$	Assigned normalized weight to x_n^i at location n	SMC	Sequential Monte Carlo		
N_s	Total number of samples	PDFs	Probability Density Functions		
S_{p}	Signal Power	XLPE	Cross-Linked Polyethylene		
N_p	Additional noise power	RMSE	Root Mean Square Error		
σ	Amplitude of computed signal	AWGN	Additive White Gaussian Noise		
N_{rms}	Amplitude of additional noise in RMS form	CDF	Cumulative Distribution Functions		
$E_{n,f}$	Difference between the true states (with modified weights) and the estimated states (without performing weight update step) at time k.	FD	Fused Data		
EDR	Energy Density Ratio	TI	Thermal Imaging		
771	.1 ' [4.0] . 1 . 0 . [т. 1	1. ' 1' . ' 1 1 1.1		

The authors in [13] presented a Super-Heterodyne ultrasonic listening-based health inspection scheme for live ABC cables in the existence of extreme, acidic environmental factors in the coastlines. The proposed method makes an essential contribution to the health inspection of ABC cables, but it is not appropriate for estimating the deterioration growth rate. The authors in [14], proposed a prognostic framework for determining the possible future deterioration development rate of functioning ABCs thermal insulation set up at shoreline regions via historical Super-Heterodyne ultrasonic listening information/data. Although this framework effectively predicts deterioration rates, the remaining useful life of operational ABC cables in coastal areas is not addressed in the current literature.

The RUL estimation of power distribution lines is essentially a key factor for planning maintenance and replacement activities in a timely manner before the actual failure. This study, for the first time, proposes the use of a multi-sensor inspection-based data fusion scheme to estimate the RUL of operational low-voltage ABC cables installed at coastal regions, improving the accuracy of the estimated results. In the reported research work, to implement a multi-sensor data fusion scheme the Super-Heterodyne Ultrasonic listening data presented in [13] is used along with the Thermal equipment-based Non-Destructive Testing (NDT) data for analysis of functional ABCs [15]. The thermal degradation of ABCs insulation as reported in [10], [11], [12], enables the use of the infrared thermography-based NDT method to acquire more data on Thermal damage in the insulation of operational ABCs set up along the coastline.

In [16], [17], [18], [19], and [20], various model-based methods for inspecting the thermal degradation process in insulated power cables are reported. These methods are finite element numerical model, Neural Network, Principal Component Analysis (PCA), mid-infrared spectroscopy, Standard Deviation Multi-Resolution Analysis (STD-MRA) representation based on Discrete Wavelet Transformers (DWT), emissivity parameter from infrared thermography. However, these approaches are not best suited for harsh and corrosive environmental



conditions, as the results are obtained through lab experiments using these models. Creating physical models that replicate these tough environmental conditions is also challenging. To address this issue, data-driven approaches are employed, utilizing actual thermal imaging-based NDT data that records all degradation-triggering factors in real-time. This method ensures a more accurate inspection of the thermal degradation process in the insulation of operational power cables.

The use of multiple sensors-based inspection modes is common in various Nondestructive Evaluation (NDE) applications [21]. The available information from multiple inspection modes can inspect the degradation trend accurately due to the information contained in multiple sensors. To effectively utilize data from multiple sensors, the development of a computationally efficient data fusion scheme is required for estimating the degradation trend when multiple measurement data is available. In [22], [23], [24], [25], [26], different data fusion schemes are reported, including neural networks, Bayesian analysis-based Dempster-Shafer evidence theory, wavelet and multi-resolution algorithms, image fusion in the time and frequency domain, and Q-transform-based techniques. All these fusion algorithms use signal processing and image processing approaches without considering the nature of a measurement process [21]. Additionally, these schemes struggle to deal with non-linear state transitions and non-Gaussian noise distributions efficiently due to their relatively high computational cost [21]. To address these issues, the authors in [21] have proposed a Sequential Monte Carlo (SMC) based Particle Filter scheme to fuse the multi-sensor NDE data using multiple NDE measurement modes.

In this paper, the authors proposed SMC SMC-based PF data fusion algorithm using multiple measurement modes "0" to estimate the RUL of live LV-ABC-Cables set up at the coastline region. This scheme is applied to fuse the actual thermal imaging and Ultrasonic testing-based NDT measurements attributing to a novel contribution in the literature. Moreover, the use of multiple sensor data improves the RUL estimation of active insulated power distribution lines mounted at the shoreline. Furthermore, the f-step prognostic framework based on PF algorithm is developed to predict the degradation trend in the operational low voltage ABC cables connected at beach areas. This approach will help power company owners perform timely maintenance and replacement activities, reducing maintenance costs and improving the reliability of power distribution networks, especially in coastal areas.

Objectives:

The goals of this research study are:

- To enhance the accuracy of estimating the future degradation growth rate in the insulation of ABC cables,
- To integrate various sensor measurement data to accurately estimate the remaining useful life of ABC cables, and
- To assess the effectiveness of the proposed algorithm in the absence of measurement data by incorporating the f-step prediction scheme with the PF algorithm.

The remaining paper is divided into five subsections. The subsequent part discusses challenges related to the problem declaration or statement, which are then addressed in the next section of the research methodology. In the research methodology portion, initially, problem formulation for an NDE-based health diagnosis scheme in terms of an iterative setup within the presence of measurement information obtained via various measuring modes will be explored. The development of a particle filter-based data fusion scheme with the assumption that the NDE measurement modes are not correlated to each other is also presented in this section. The implementation of Principal Component Analysis (PCA) to legalize our assumptions of independence of measurement modes is then discussed in the same section. In the end, an overview of the findings and conclusions is covered.



Research Methodology:

In this section, we described the problem formulation of RUL estimation in terms of Bayesian estimation problem. Moreover, the historical databases in terms of percentage degradation in the insulation of energized ABCs installed in coastal areas using two different NDT schemes are presented. We also discussed the application of PF algorithm for multi-sensor data fusion. Finally, the execution procedure for the PF-based f-step forecasting approach as well as the step error evaluation technique are demonstrated.

Problem Formulation:

The problem formulation applies to RUL estimation of in-service power distribution lines with multiple measurement modes **O**. The problem of RUL estimation in live power cable is similar to the defect growth in cable insulation in the context of percentage degradation w.r.t intervals (i.e. the total number of weeks). In this case, the time interval is divided into N locations. The information about the defect growth is unknown at each discrete location. The defect growth in cable insulation is expressed in terms of $\vec{X} = \{x_1, x_2, x_3, ..., x_n\}$, where each element $\mathbf{x}_{\mathbf{n}}$ of the set is stated (degradation growth) at the discrete location $\mathbf{n}(1 \leq \mathbf{n} \leq \mathbf{N})$. We assumed that measurements $\overline{z}_n=\{z_n^1,\,z_n^2,\,\dots$, $z_n^o,\,\dots$, $z_n^o\}$ = $\{\,z_n^o|o=1:0\}$ from Omeasurement modes are known at each position index $n (1 \le n \le N)$ [27]. Due to degradation, including fractures in cable insulation, and the unavoidable noise in nondestructive testing (NDT) measurements are stochastic, a statistical framework methodology is used to estimate defect growth with Bayesian approaches [28]. This Bayesian estimation problem can be reformulated as a statistical estimation challenge, as described in references [21], [29]. In this a series of states (unidentified parameters), $\{z_1^1, z_1^2, \ldots, z_1^0, z_2^1, \ldots z_n^0, \ldots z_n^0\}$ represents the associated precise measurements. The posterior PDF $\mathbf{p}(\mathbf{\vec{X}}|\mathbf{\vec{Z}})$ could be represented as a Bayesian evaluation issue. for every $\mathbf{0^{th}}$ measuring mode along with \vec{X} states. Also, \vec{X} states can be determined via the posterior PDF $p(\vec{X}|\vec{Z}) \propto p(\vec{Z}|\vec{X})p(\vec{X})$, in which $p(\vec{Z}|\vec{X})$ indicates a likelihood function and then $\mathbf{p}(\mathbf{\vec{X}})$ is a previously acquired knowledge of $\mathbf{\vec{X}}$ states. Estimating the likelihood function has been costly in terms of computation. To solve this issue, generate the posterior PDF in a series of values at every position over n places. This will decrease both computational expenses as well as complexity [30]. The exponential density is used as a prior density

$$p(x_n|x_j|_{\substack{j \in N_n \\ j \neq n}}) = e^{-\sum_{j \in N_n} \frac{\left\|x_j - x_n\right\|^1}{i}},$$

Where i must be selected around 1 to reduce the variability in x_n state within the N_n neighborhood, and $x_j|_{j\in N_n}$ are the states in N_n of 'n' location.

In this section, we have discussed the Bayesian estimation problem as a tracking problem. The Bayesian estimation problem [28] can be represented by the state transition equation to model the state x_n at each 'n' location: $x_n = f_n(x_j|_{j \in N_n}, v_n) \leftrightarrow p(x_n|x_j|_{j \in N_n})$, and measurement $x_n = f_n(x_j|_{j \in N_n}, v_n) \leftrightarrow p(x_n|x_j|_{j \in N_n})$

model to relate the z_n to the x_n states: $z_n = h_n^o(x_n, \mu_n^o) \leftrightarrow p(z_n|x_n)$, where f_n is the state transition process, h_n^o is the measurement process, v_n is the process noise, and μ_n^o is the measurement noise. To connect the x_n and z_n measurements, we took into account a polynomial-based measurement framework similar to the one described in reference [27] to relate x_n with z_n measurement: $z_n = \sum_b^B c_b x_n^b$, where: 'c' represent a polynomial figure extracted via a measurement repository or database. The above model has a minimal computational complexity of B^{th} order. Both the state transition as well as measurement



framework illustrate a tracking (or chasing) problem or issue [31]. In the context of tracking of the target scenarios [31], the function: $f_n(x_j|_{j\in\mathbb{N}_n}, v_n)$ computes the target's movement from

the x_j location, while $h_n^0(x_n, \mu_n^0)$ identifies the target location. The most effective approaches for chasing (or tracking) issues are currently Kalman-filtering and particle-filtering [30], [32] (which are described more thoroughly in the subsection).

Super-Heterodyne Ultrasonic Listening-Based Historical NDT Data Base:

The authors in [33], presented a detailed description of capturing the progressive damage within the thermal insulation of installed ABCs via field-acquired Ultrasonic listening based NDT data using Hilbert Huang Transform (HHT). Briefly, HHT scheme performs two steps including Empirical Mode Decomposition (EMD), and Hilbert Huang Transform (HHT). The EMD scheme breaks the non-linear and non-stationary signals into high to low-frequency components called Intrinsic Mode Functions (IMFs). The major information of the original signal is present in the first three IMFs [34], [35]. The HHT was applied on the first three IMFs to obtain the Hilbert or energy graph/spectrum. Figure 1 depicts the energy graph also known as Hilbert-Spectrums of working and failed cables set up at different sites of metropolis Karachi [33]. The two Regions of Interest (ROI) are selected in HHT spectrums as shown in Figure 1. The Average Energy Density Ratios (Avg. EDR) for ROI A and ROI B were calculated in [13]. In this study, the delta EDR (ROI A – ROI B) is used to make the Ultrasonic listening-based historical database in terms of percentage degradation to estimate the RUL of live ABC cables.

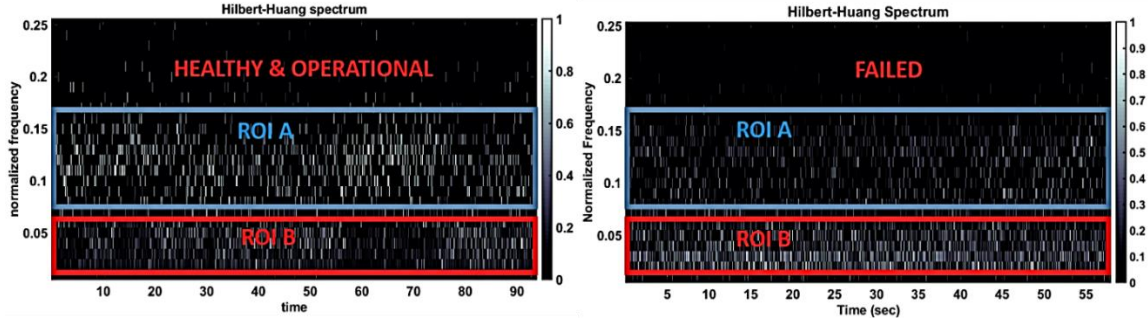


Figure 1: HHT Spectrum Evaluation of Active and Defective Cables [1] **Table 2:** Degradation Rate of Live ABC cable using ΔEDR_{new}

Cable Status	Date	ΔEDR	$\Delta EDR_{new} =$	Degradation
Cable Status			$(1-\Delta EDR)$	(%)
	13-Jul-2018	0.363	0.637	13.58641359
	7-Aug-2018	0.322	0.678	17.68231768
	20-Oct-2018	0.29	0.71	20.87912088
	4-Nov-2018	0.271	0.729	22.77722278
Healthy (Used), Site-I	01- Dec-2019	0.26	0.74	23.87612388
	08-Jan-2019	0.241	0.759	25.77422577
	19-Mar-2019	0.141	0.859	35.76423576
	25-Apr-2019	0.106	0.894	39.26073926
	5-Jun-2020	-0.189	1.189	68.73126873
Healthy (New), Site-II	25-Jan-2019	0.499	0.501	0
Faulty, Site-III	23-Oct-2018	-0.502	1.502	100

In Table 2, the delta EDR presented in [13] is tabulated in column three. The delta EDR_{new} is obtained by subtracting the delta EDR from 1. The percentage degradation is calculated using (1)

Degradation (%) =
$$\frac{\Delta EDR_{new}^{current} - \Delta EMD_{new}^{min}}{\Delta EMD_{new}^{max} - \Delta EMD_{new}^{min}}$$
 (1)



Where $\Delta EMD_{new}^{current}$ is the present value of delta EDR_{new} , ΔEMD_{new}^{min} is the minimum value of delta EDR_{new} with zero percentage degradation when new ABC cable was installed on 25th Jan 2019, and ΔEMD_{new}^{max} is the maximum value of delta EDR_{new} with 100% degradation in faulty cable on 23rd Oct 2018.

Data Collection Using Ultrasonic Probe Testing Gun:

The field-acquired data was collected from July 2018 to June 2020 (a total of 730 days). The data is estimated up to 1200 Days over 7 days via the Cubic-Spline-Interpolation (CSI) based approach. The obtained database is used for the RUL estimation of ABCs. These results are shown in Figure. 6 and are discussed in detail in section 3.

Infrared Thermography-Based Historical NDT Data Base:

This section involves the application of different procedures to identify the damage to the ABCs insulation under harsh corrosive environmental conditions using thermography. These include infrared thermography, image segmentation, data normalization, histogram computation, cumulative distribution function, and 90 % CDF value of maximum temperature. Infrared thermography is widely used in the diagnosis and predictive-based maintenance of active and operational electrical equipment [36], [37], [38], [39].

The health and condition of the equipment were inspected with the help of pixel intensity present in the thermal image. In this study, a thermal imaging scheme was considered to measure the change in the temperature distribution in the insulation of live ABCs. In Figure 2, a thermal image of active low-voltage ABC is depicted. In [40], the authors reported that background data is not required in the thermal image analysis.

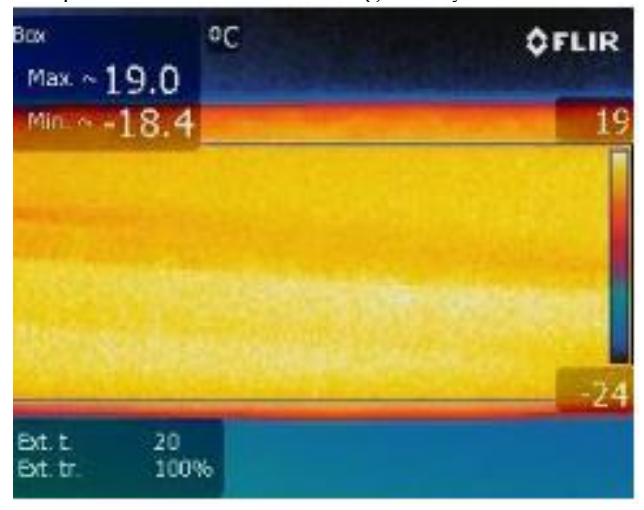


Figure 1: Energized ABC Thermal Image

There are different segmentation categories including region-based, threshold-based, and edge detection-based segmentation [41], [42]. The most widely used segmentation scheme is thresholding segmentation, which contains two subcategories including local thresholding and global thresholding. In threshold-based segmentation, all the pixels are divided into groups based on fixed threshold selection criteria. In this study, global thresholding segmentation was used to select the ROI from the field-acquired thermal imaging data of energized ABCs. This was achieved by assigning a value of 1 to all pixels that exist in the ROI and have high-temperature readings. All the pixels outside the ROI are set to zero. The Eq. (2) is used to convert the thermal images of ABCs into binary configuration [40], [41].

$$w(u, v) = \begin{cases} 1, & j_i(u, v) > t_{Otsu's} \\ 0, & j_i(u, v) < t_{Otsu's} \end{cases}$$
 (2)

Where w(u, v) is obtained segmented image matrix, $j_i(u, v)$ is the i^{th} pixel in the thermal image matrix j(u, v), and $t_{Otsu's}$ is the Otsu's threshold level according to which pixels



are selected. The Otsu's thresholding technique is used to optimize the threshold value $t_{Otsu's}$ using the variance between the clusters [41]. Figure 3 illustrates the process of selecting the required ROI using global thresholding segmentation [15]. Figure 3(a) shows the original raw image of an active LV-ABC-cable. Figure 3(b) is the segmented image, where the white region is the required ROI and the black area is the background. Figure 3(c) is the final obtained segmented image of energized ABCs using Eq. (3)

$$b(u_i, v_i) = j(u_i, v_i) \times w(u_i, v_i)$$
(3)

Where $b(u_i, v_i)$ is the final segmented image matrix with required pixels exist in the ROI, $j(u_i, v_i)$ is the original image matrix, and $w(u_i, v_i)$ is the segmented matrix obtained using Eq. (2). The ABC insulation is thermally degraded over time due to which the temperature measurements in each acquired thermal image vary concerning time. This variation was removed by applying the min-max normalization technique to the obtained segmented matrix b(u, v) [43]. The Eq. (4) is used to apply the min-max normalization method.

$$b'(u_i, v_i) = \frac{b(u_i, v_i) - \min(b(u, v))}{\max(b(u, v)) - \min(b(u, v))}$$
(4)

Where $b'(u_i, v_i)$ is the i^{th} pixel in the normalized segmented image matrix b'(u, v), and b(u, v) is the segmented matrix with variation in the pixel value. To analyze the change in the thermal energy distribution of ABC insulations, histogram computation using the normalized segmented thermal data is presented in the reported work. The total energy under each histogram is normalized to 1. To measure and quantify the shift in the energy distributions of thermal data, various statistical parameters including mean, standard deviation, coefficient of variation, entropy, skewness, and kurtosis are examined. However, the trend of statistical parameters was not suitable for the analysis. Similarly, Cumulative Distribution Functions (CDFs) are used to make the historical database of field-acquired thermal images of energized ABCs in the presented work. An esteemed trend was observed in the normalized thermal energy values at 0.9 CDF. In Table 3, normalized thermal energies of operational ABCs installed in coastal area at 0.9 CDF are tabulated.

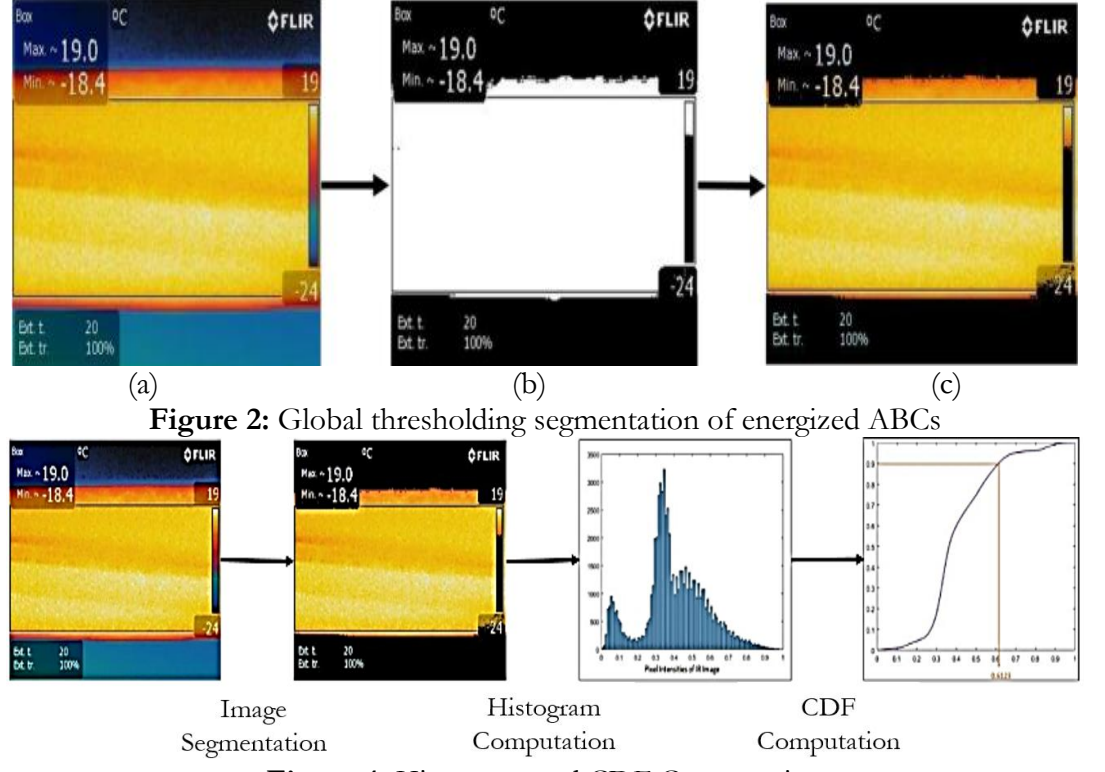


Figure 4: Histogram and CDF Computation



The percentage degradation is calculated using Eq. (5) and is tabulated in Table 3. Figure 4 shows the key steps of all procedures [15].

Degradation (%) =
$$\frac{0.9 \text{ CDF}_{\text{current}} - 0.9 \text{ CDF}_{\text{min}}}{0.9 \text{ CDF}_{\text{max}} - 0.9 \text{ CDF}_{\text{min}}}$$
(5)

Where 0.9 CDF_{current} is the current value of normalized thermal energy of pixels at 90% CDF, 0.9 CDF_{min} is the minimum value of normalized thermal energy of pixels at 90% CDF with zero percentage degradation when the new ABC cable was installed on 25th Jan 2019, and 0.9 CDF_{max} is the maximum value of normalized thermal energy of pixels at 90% CDF with 100% degradation in faulty cable on 23rd Oct 2018.

Data Collection Using Thermal Imaging Camera:

The field-acquired data was collected from July 2018 to June 2020 (a total of 730 days). The data is estimated up to 1200 Days with an interval of 7 Days using the CSI technique. The obtained database is used for the RUL estimation of ABCs. These results are shown in Figure. 6 and are discussed in detail in section 3.

Table 3: Degradation Rate of Live ABC cable Using 0.9 CDF

Cable Status	Date	0.9 CDF	Degradation (%)
	13-Jul-2018	0.6615	14.08765653
	7-Aug-2018	0.6874	25.67084079
	20-Oct-2018	0.7034	32.82647585
	4-Nov-2018	0.7067	34.30232558
Healthy (Used), Site-I	01- Dec-2019	0.7331	46.10912343
	08-Jan-2019	0.7412	49.73166369
	19-Mar-2019	0.7438	50.89445438
	25-Apr-2019	0.7452	51.52057245
	5-Jun-2020	0.82	84.97316637
Healthy (New), Site-II	25-Jan-2019	0.63	0
Faulty, Site-III	23-Oct-2018	0.8536	100

In the next sections, two different types of databases in terms of percentage degradation growth rate, are formed. These databases are fused, using PF based multi-sensor data fusion scheme, which is described in the upcoming section.

Application of Particle Filters Using Multiple Mode Measurement Data:

The authors in [30], and [32] reported that the optimal solution to the tracking problem is the Kalman filtering, but it is only applicable when the state transition function and measurement functions are linear with Gaussian noise distributions. On the other hand, deficiencies development in tiny structures constitute an irregular behavior, and noise variations may be non-Gaussian (multidimensional). Sequential Monte Carlo (SMC) based Particle Filtering methods are applied to solve Bayesian estimation problems with non-linear state transition models and non-Gaussian noise distributions [27].

Theory of Particle Filters:

In SMC-based Particle Filters, the probability densities are represented in terms of particles. This type of representation applies to any state-space model [29], [31]. In this scheme, the posterior pdf is recursively obtained based on all available information. Now, a brief working of PF algorithm is presented next. A specific measurement mode known as a single-measurement-mode (i.e., O = 1) has been chosen for ease of use, and $\overline{z}_n = \{z_n^o \mid 0 = 1\} \equiv z_n$ are the measurements obtained via a single measurement. This selection will be removed in the next section, where the PF framework will be extended to integrate the multimodal measurements. Within a single evaluation or measurement setting, a PDF of the state x_n conditioned on every data from measurements to the value $p(x_n, z_{1:n})$ and involving z_n might be witnessed gradually within 2 stages: forecasting along with weight revision step. The state



transition model is employed to forecast the Probability Density Function (PDF) from the current measurement location to the subsequent location. The state transition model connects states within a neighborhood. Consider the n-1 separate location has the specified PDF $p(x_n|z_{1:n-1})$. As already stated, the system model is employed to forecast the PDF of the state x_n employing the Chapman-Kolmogorov equation [30], which is presented as

$$p(x_n|z_{1:n-1}) = \int p(x_n|x_{n-1})p(x_{n-1}|z_{1:n-1}) dx_{n-1}$$
 (6)

We could adopt the Markov mechanism of order one, then the posterior PDF of the state x_n will become $p(x_n|x_{n-1}, z_{1:n-1}) = p(x_n|x_{n-1})$. Because of the unidentified disruptions, the state is expressed as random noise. The probability density function is distorted and weakened during the particle filter technique's forecasting step. The updating step uses the most recent information to estimate the PDF. In the weight revision step, Bayes' theorem is applied in the following manner:

$$p(x_n|z_n) = \frac{p(z_n|x_n)p(x_n|z_{1:n-1})}{p(z_n|z_{1:n-1})}$$
(7)

The desired posterior likelihood density on every n^{th} place is stated as samples and weights. At this point, we'll go over the fundamentals of the technique in depth. We took into consideration the random measure $\{x_n^i, w_n^i\}_{1:N_s}$ for defining the subsequent pdf at n distinct locations. Whereas x_n^i , w_n^i is an array of supporting points as well as their corresponding measurements, we have determined the total quantity of samples as $i=1:N_s$. Weight adjustment has been defined as $\sum_{i=1}^{N_s} w_n^i$. So at n positions, the pdf could be identified as [28]

$$p(x_n|z_n) \approx \sum_{i=1}^{N_S} w_n^i \delta(x_n - x_n^i)$$
 (8)

Adjusted weights are determined using the importance sampling principle [29]. This rule can be expressed using a PDF such that $p(x) \propto \pi(x)$ where it is difficult to obtain elements (or data points), but $\pi(x)$ can be accurately calculated and elements can be produced via $\pi(x)$. Comparably we can suppose x^i to be sampling data that are likely to be quickly produced via proposal density q(.), referred to as importance density. Weights of density p(x) can be approximated from $\sum_{i=1}^{N_s} w^i \delta(x-x_n^i)$. Where $w^i \propto (\pi(x^i)/q(x^i))$ is the normalized weight of the i^{th} particle. After accepting the measurement z_n at n^{th} separate location, we aim to estimate $p(x_{1:n}|z_{1:n})$ using an entirely novel particle group. In a similar way the set of weights w_{n-1} are supplied to position n-1, and can be determined via the weight (or measurement) updated equation. The measurement updated equation is obtained from the principle of importance sampling in the following manner:

$$w_n^i \propto w_{n-1}^i \frac{p(z_n | x_n^i) p_{N_s}(x_n^i | x_{n-1}^i)}{q(x_n^i | x_{n-1}^i, z_n)}$$
(9)

The Sampling Importance Replication procedure was first described in references [28], [30], consequently the importance density associated with the SIR technique can be $q(x_n^i|x_{n-1}^i,z_n)=p(x_n^i|x_{n-1}^i)$. Therefore, from $w^i \propto (\pi(x^i)/q(x^i))$ and (9), the following is derived,

$$w_n^i \propto p(z_n|x_n^i) \tag{10}$$

The SIR variant of PF uses the preceding density $p(x_n|z_n-1)$ to determine the importance of density [27]. The preceding density described in Equation (11) is assumed to follow an exponential distribution [44]. In the currently available research, multiple distributions including lognormal, Weibull, and exponential have been utilized for modelling life distributions



[45], [46], [47]. As the profile variable β comes towards 1, the Weibull distribution merges to an exponential distribution with an unvarying failure/hazard quantity. As a result, it was used in the present investigation to more accurately forecast degradation rates [45], [47].

$$p(x_n|x_{n-1}) = e^{-\frac{\|x_n - x_{n-1}\|^a}{a}}$$
(11)

The parameter a is a single value that regulates the variability in the predicted results (states x_n). The measurement model establishes a connection between states and measurements, essential for computing the chance or likelihood of the specimens generated by using the prior or previous density. We handled the rate of deterioration development as an obvious occurrence of state variables x_n with random noise n_n being the sole source of ambiguity. Measurements are obtained immediately based on true states, as in [29],

$$y_n = f(x_n, n_n) \tag{12}$$

The measurement model can be represented in the form of Dth order polynomial, as illustrated here:

$$y_n = \sum_{d=1}^{D} c_d x^d \tag{13}$$

The d^{th} order coefficient c_d associated with the polynomial could be established by using the present states x^d from the database as well as the related measurements [44]. Weight assignment and revision are done via the likelihood of the probability density function (PDF), as illustrated in Equation (9). This probability is determined by the distinction between real measurement information and the estimated information employing samples (particles) and the measurement model, which is then utilized for assigning weights to the specimens. Since future state measurement data is unavailable, updates are restricted to the existing states, allowing only the Particle Filter's prediction step to be executed. The absence of the update step results in an error in computing the posterior PDF. The magnitude of this error is directly influenced by the duration (number of days) without the update step.

Particle Filtering for Multi-Sensor Data Fusion:

When there are multiple measurement modes, the likelihood probability density functions (PDFs) for each mode must be taken into account when assigning weights to the samples. Let $\mathbf{w}_{n}^{i,o}$ represent the weight of sample i at position index n assigned by the individual measurement mode o. For each sample at every position index, o weights are computed using the respective likelihood PDFs. The likelihood function for the oth measurement mode is defined by Equation (10) and the following:

$$w_n^{i,o} \propto p(z_n^o | x_n^i) \tag{14}$$

We assumed that the measurement processes are independent, for that the joint likelihood for measurement modes o = 1, 2, ..., 0 is the product of the likelihood for each measurement mode, as follows:

$$p(z_n|x_n^i) = p(z_n^1|x_n^i), p(z_n^2|x_n^i), \dots, p(z_n^0|x_n^i)$$
(15)

Therefore, from (14) and (15), we get the following:

$$w_n^i \propto p(z_n^1|x_n^i), p(z_n^2|x_n^i), \dots, p(z_n^0|x_n^i)$$
 (16)

Using (10) and (16), the final weight assigned to sample i at position index n is as follows:

$$w_n^i \propto w_n^{i,1}, w_n^{i,2}, \dots, w_n^{i,0}$$
 (17)

As mentioned earlier, it's assumed that the measurement processes are independent. However, there might be correlations among them, invalidating this assumption. To address this, Principal Component Analysis (PCA) is employed on data from different measurement



modes. PCA is a mathematical technique that transforms data into a new coordinate system in an orthogonal manner [48], [49]. It can be applied to data from multiple measurement modes. For each position index n, measurements $\mathbf{z_j^{1:0}}|_{\mathbf{j}\in M_n}$ within its neighborhood from all measurement modes (1: Q) are considered. These multidimensional data then undergo PCA. The following steps outline the evaluation of the principal components:

- The multi-sensor measurements $z_j^{1:0}|_{j\in M_n}$ are stored as vector $v^0|_{o=1:0}$, where each measurement mode is assumed to be one component of the vector.
- The data vector is adjusted by subtracting out its mean given by:

$$v^{0} = v^{0} - \text{mean}(v^{0})$$
 (18)

• The adjusted data vectors are arranged as rows of a matrix. This newly formed matrix will be called the "adjusted data matrix," given as

$$v = [v^1, v^2, \dots, v^0]$$
 (19)

• The covariance matrix of the "adjusted data matrix" is computed as follows:

$$\sigma^0 = \text{cov}(\mathbf{v}^0) \tag{20}$$

• Eigenvectors λ^0 of the covariance matrix are then evaluated as follows:

$$\lambda^{0} = \operatorname{eig}(\sigma^{0}) \tag{21}$$

• The computed eigenvectors are organized as rows in a new matrix. This matrix is termed the "feature matrix" as follows:

$$\lambda^{0} = \lambda^{1}, \lambda^{2}, \dots, \lambda^{0} \tag{22}$$

• Finally, the "feature matrix" is multiplied by the "adjusted data matrix"

$$\psi = \lambda v \tag{23}$$

The rows of the resulting matrix ψ represent the principal (uncorrelated) components in the data as follows:

$$\psi = [\psi^1, \psi^2, \dots, \psi^0] \tag{24}$$

The resulting components ψ^0 have no relationship with one another. The PCA methodology produces separate data having O dimensions. These distinct components are subsequently interpreted as data from different measurement modes.

Implementation:

The process for evaluating the posterior probability density function (pdf) of the state (flaw depth) is illustrated in Figure 5 and summarized as follows:

- Initialization: N_s samples are drawn at each position index from the prior pdf, as defined in Equation (11).
- Weight Assignment: Weights are assigned using the likelihood pdf, as described in Equation (9). This pdf is determined by the error between the computed measurement using the measurement model and the actual measurement. If the difference between computed and actual measurements for a sample is small, the sample's weight is high, and vice versa.
- The Measurement Model: This model establishes the relationship between the state and measurements. It is derived from a training database of known states and corresponding nondestructive evaluation (NDE) measurements, as given in Equation (13). The coefficients of the polynomial c_d are determined from this training database.

During resampling, particle filters often encounter a problem known as degeneracy [50]. This occurs when, after a few iterations, only one particle retains significant weight, rendering



the others negligible. The resampling process aims to address this issue by discarding particles with small weights and focusing on those with larger weights. This ensures that the posterior probability density functions (pdfs) are estimated at all locations. The estimated samples are assembled with uniform weights to determine a posterior PDF of a single position (for n = 1). Keep doing the steps for computing the posterior PDF $\mathbf{p}(\vec{\mathbf{X}}|\vec{\mathbf{Z}})$ at all positions (such as, for all 'n' values. The assumption of independence among measurement modes forms the basis of the proposed particle-filter-based data fusion technique. Since the output of the PCA technique consists of uncorrelated components, this transformation reinforces the validity of assuming independence among measurement data.

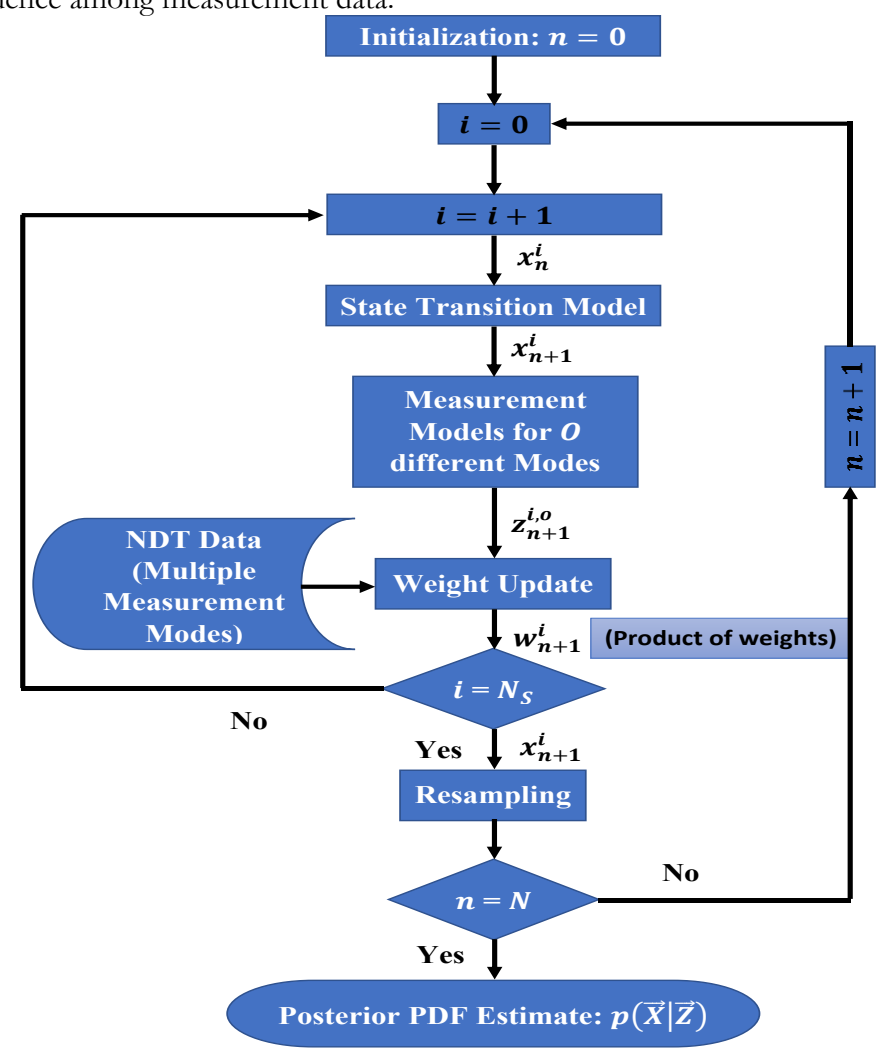


Figure 5: Particle filter-based multi-sensor data fusion scheme Particle Filter-Based f-Step Prediction Schemes:

The f-step prediction schemes reported in [14], and [46] are also proposed in this study to perform the future degradation growth rate estimation. This scheme is implemented on the historical database obtained from all the reported methods in this study, including ultrasonic listening-based NDT, thermal imaging-based NDT, and PF algorithm-based multi-sensor fusion. In this paper, only 1-step to 2-step predictions are performed.

• 1-Step: At this stage, f is equal to 1, which means the prediction step for the 2nd sample/state is performed using all the information of the 1st sample/state. In the subsequent phase, the weight of the second state has been modified and all of the



information obtained from the second state will be utilized to forecast the number three state.

• **2-Step:** At this phase, f equals 2, which means the prediction step for 3rd sample/state is performed using all the information of 1st sample/state. In the subsequent phase, the weight of the second state has been upgraded, and all the information gathered from the second state/sample will be utilized to predict the number of fourth states.

The new results are generated using PF-based 1 to 2-step forecasting schemes and are used to compare the actual and predicted states. This difference is used to identify the weight of the small particle and forecast the next sample/state. The approach sequentially strengthens itself during each subsequent iteration.

Step Error Analysis:

The inaccurate predictions were caused by lacking a revision step within the state transition framework, as stated in reference [46]. To address this issue, the algorithm computes the distinction between estimated and true states. This is done by calculating the error $E_{n,f}$ until its present level n [49], whereas f symbolizes the entire amount of essential future suggested states ($f = 1, 2, 3, 4, 5 \dots, F$). The step error estimation technique adopts the following steps:

- Step 1: Predict the total of F states for the very initial time moment (each moment represents roughly seven days).
- **Step 2:** Modify the weight of the forecasted state.
- At the very initial moment, employ appropriate measured values to determine the upcoming F states (overall states: 1 + F) via the forecasting step.
- While at the subsequent moments or time instant, apply the collected precise measurements to determine the subsequent states (overall states: 2 + F).
- Continue this process for N days (up to the accessible measurement information) and forecast future outcomes F states (overall states: N + F).

The method described previously offers state information at all N moments either using the revised weight (u^*) and along with a revised weight (\hat{u}). The distinction among both of these two states delivers an incorrect value for "n" moments via "f" varying between 1 to F. The margin for error could be determined as follows:

$$E_{n,f} = (u_{n+f}^* - \hat{u}_{n+f}) \mid_{f=1}^{F} \mid_{n=1}^{N}$$
 (25)

Equation (25) is further detailed in equations (26) to (27). While exploring the approach used for calculating the f-step error evaluation approach, whenever the initial state is modified (n = 1), the error rate can be calculated as the distinction among the expected $1+f_{th}$ state and the updated f_{th} state (f steps ahead). Furthermore, when the subsequent state (i.e., n = 2) is modified, the margin of error is the difference among the predicted $2+f_{th}$ state and the modified/updated $2+f_{th}$ state, and it continues. The error rates in the forecasting results (deterioration development rate) have been obtained for values of f which are to 1 or 2, via the following equation:

$$E_{n,1} = (u_{n+1}^* - \hat{u}_{n+1}) \mid_{n=1}^{N}$$
 (26)

$$E_{n,2} = (u_{n+2}^* - \hat{u}_{n+2}) |_{n=1}^{N}$$
 (27)

Equations (26) to (27) represent the series of prediction errors for "f" steps. The effectiveness of the prognostic scheme proposed in this study is evaluated in terms of root mean square error (RMSE). Equation (28) has determined the value of the RMSE for the "f" step estimation error series framework using the following formula:



RMSE =
$$\sqrt{\frac{1}{S} \sum_{n=1}^{S} E_{n,f}^2}$$
 (28)

In Equation (28), S refers to the total number of estimated states applied by the f-step estimation process (i.e., S is 170 for 1-step estimation and 169 for 2-step estimation). $E_{n,f}$ indicates the distinction between the real and expected states at instant/moment n (such as f = 1 and f = 2). Inaccuracies in the forecasting steps, expressed as RMSE, were calculated via Equations (26) to (28), and are presented in Table 5. A detailed analysis of these errors will be discussed in the third section.

Data Collection and Description:

Super-Heterodyne Ultrasonic Listening Data:

The detailed data description is reported in [13], [33]. The present study uses an ultrasonic testing gun to capture corona emission signals to identify the insulation rupture of ABC cables. The test gun is recognized as the UE Systems© Ultra probe® 9000. Subsequently, this study uses it for listening to super-heterodyned ultrasonic corona discharge signals around the vicinity of live ABC cables. The Ultra probe® 9000 translated the ultrasonic emissions from (20 kHz - 100 kHz) into the audible region (i.e., 20 Hz - 20 kHz), making it detectable by the human ear. The detectable signatures were initially evaluated with noise-reducing headsets. The received super-heterodyned information is detected in the form of a hissing noise, known as corona discharge, and then saved on a laptop computer. An ultrasonic signal was recorded along a 45-meter length of ABCs (i.e., for fixed segments). To reduce the effects of air instability, a rubber cone was incorporated into the Ultra probe.

The ultrasonic listening data was acquired periodically from operational ABCs installed at three different locations of metropolis Karachi including South City Hospital, Beach View, and Al-Shifa Hospital. These locations are categorized as Site-I, II, and III. The first ultrasonic measurement was recorded on 13th July 2018. The prior service life of the used ABC cable installed at Site-I was 119 weeks (or 833 days) [13]. The new cable was installed at Site II on 25th January 2019. Similarly, the faulty ABC cable was reported on 23rd October 2018 at Site-III. The total service life of faulty cable installed at Site-III was 277 weeks (1939 days or 5.312 years) and the prior service life of Site-I ABC cable was 190 weeks (833 days or 2.282 years) [13]. In this study, the total service life of ABC cable installed at Site-III is used as a reference for the comparison of total service life achieved using different databases. The comparison of total service life of faulty ABC cable at Site-III in terms of percentage error is shown in Table 4. The R_U is the remaining useful life (starting from the date of the first ultrasonic measurement i.e. 13th July 2018) of live ABC cable at Site-I. In Figure 6, the percentage degradation plot of live ABC at Site-I is shown using a Super-heterodyne NDT measurement-based historical database.

Thermal Imaging Data:

A detailed description of the data is reported in [15]. Briefly, the useful life of ABCs in coastal areas is less as compared to non-coastal areas. Therefore, coastal belt areas of the metropolis Karachi including Site-I, II, and III are selected to acquire field data. The FLIR E40-thermal imaging camera is used to capture the temperature-energy distributions produced in the operational ABCs insulation. A distance of 5 to 6 inches was maintained between the camera and ABC cable, to reduce the effect of atmospheric conditions. The "Lava" palette mode and a temperature range from 20 degrees to 120 degrees were selected before each measurement. The data acquisition was performed at night, to avoid the effect of sunlight. The faulty cable at Site-III was kept energized at the time of data acquisition.

Table 3 presents the percentage degradation in active ABC cables using thermal imaging. Initially, the percentage degradation was recorded for 710 days with a 30-day interval. The CSI



scheme was employed to interpolate additional data points between the available states within the database. As a result, data for 1200 days with a 7-day interval is now available, resulting in 171 samples per state from 1 to 1200 days. In Table 4, the estimated service life of ABC cable at Site-I using a thermal imaging scheme is presented (1709 days/4.282 years). Similarly, the percentage error between the total service life estimated using thermal imaging and the actual total service life of the faulty ABC cable at Site-III is presented in Table 4. In Figure 6, the percentage degradation plot is shown using the thermal imaging NDT historical database.

Table 4: Rul Estimation of Active ABC Installed At Site-I

Database	RUL (R _U)	Prior Service Life in Days (R _P)	Estimated Total Service Life in Days ($L_E = R_U + R_P$)	$\frac{\frac{l_F - L_E}{L_E} \times 100}{\left \frac{L_F - L_E}{L_E} \right \times 100}$
Thermal Imaging	876	833	1709 (4.682 years)	13.458
PF-Fusion	1072	833	1905 (5.2 years)	1.75
Ultrasonic Listening	1200	833	2033 (5.569 years)	4.623

The Particle filter-based multi-sensor data fusion scheme using multiple measurement modes is applied to the actual Ultrasonic listening database and thermal imaging database. A total of 1000 samples per instant are used to implement the PF-based data fusion algorithm. The resulting estimated percentage degradation in the insulation of live ABC at Site-I is compared with the actual percentage degradation. This actual degradation growth in terms of percentage is obtained from field-acquired data using Ultrasonic probe listening and Thermal Imaging NDT measurements. In Table 4, the comparison of the actual service life (of faulty ABC at Site-III) and the estimated total service life of ABC cable at Site-I using multiple measurement modes is presented. Figure 6 presents a percentage degradation plot using a pf-based data fusion scheme. Additionally, the pf-based f-step prediction scheme is applied to estimate the future degradation growth rate in live ABC cable.

The same number of samples are utilized for implementing the proposed PF-based data fusion scheme. The second-order polynomial measurement function has been chosen due to its ease of use and low complexity. To assess the algorithm's effectiveness, we put additive white Gaussian noise (AWGN) into the sensor measurement data. AWGN models various random processes [51], to take into consideration the effect of inserted noise, we estimated the Signal-To-Noise Ratio (SNR), which can be described as the ratio of the derived signal power S_P to the AWGN power N_P:

$$SNR = \frac{S_P}{N_P} = \frac{\sigma^2}{N_{rms}^2}$$
 (29)

Here, σ and N_{rms} indicate the magnitudes of both the calculated signal and unwanted noise in RMS form, subsequently. For our case study, the SNR value is set to 10. In the present investigation, we have used 1000 samples (N_s) for each location. Since noise can degrade the performance of the PF algorithm, f-step error analysis is conducted using the actual and predicted states, measured in terms of root mean square error (RMSE).

Results and Discussion:

This section presents the evaluation of the performance of the proposed Particle Filter (PF)-based multi-sensor data fusion scheme for estimating the Remaining Useful Life (RUL) of live Aerial Bundled Cables (ABCs) in coastal areas such as the metropolis of Karachi.

Discussion:

Figure 6 represents percentage plots for damage increase in the thermal insulation of live ABC cable placed at Site I. The actual historical databases were made using Ultrasonic listening and Thermal imaging-based NDT measurements. The actual states using thermal imaging (i.e.

Actual States TI) were plotted up to 1200 days with an interval of 7 days. The estimated remaining service life (R_{II}^{TI}) of ABC cable at Site-I using Thermal imaging data is 876 days, which starts from the first thermal imaging-based NDT measurement (i.e. 13th July 2018), and it is depicted in Figure 6. In this process, we have estimated the RUL of active ABC installed at Site-I only. In Table 4, the total prior service life (R_P) of ABC cable at Site-I is given, which is 833 days. The total estimated service life (L_F^{II}) of ABC using a thermal imaging database is 1709 days (or 4.682 years). The actual service life of faulty (L_F) ABC cable at Site-III is given (1939 days or 5.312 years). The estimated service life (L_E^{TI}) of the active ABC cable at Site-I, determined using thermal imaging data, is compared to the actual service life of the faulty ABC cable at Site-III in terms of percentage error. In Table 4, the obtained percentage error is given as 13.458%. This indicates that the remaining useful life of active ABCs installed in coastal areas, estimated using thermal imaging-based temperature-energy distributions, has an accuracy of 86.542%. Similarly, the actual states using Ultrasonic listening-based testing (i.e. Actual States UT) are plotted up to 1200 days with an interval of 7 days. The estimated remaining service life (R_{U}^{UT}) of ABC cable at Site-I, using UT data is 1200 days, which starts from the first Ultrasonic listeningbased NDT measurement (i.e. 13th July 2018), as depicted in Figure 6. The total estimated service life (L_F^{UT}) of ABC using the Ultrasonic listening database is 2033 days (or 5.569 years). The estimated service life (LET) of active ABC at Site-I is compared with the actual service life of faulty (L_F) ABC cable at Site-III in terms of percentage error. The obtained percentage error is 4.623% (or 95.377% accuracy) and is tabulated in Table 4.

The plot of degradation growth (in terms of percentage) in the insulation of active ABC at Site-I using the proposed particle-filter-based multi-sensor data fusion scheme is also shown in Figure 6. A total 1000 number of samples were used for the implementation of the proposed scheme. The historical database of Ultrasonic listening and Thermal Imaging measurement methods were fused using Equations (17), (23), and (24) in the particle-filter implementation. In Figure 6, the actual states using the proposed PF-fusion scheme (i.e. Fused States) are plotted up to 1200 days with an interval of 7 days. The estimated remaining service life (R_U^{Fusion}) of ABC cable using the PF-fusion scheme is 1072 days, which starts from the first thermal imaging-based NDT measurement (i.e. 13th July 2018). In Table 4, the total estimated service life (L_E^{Fusion}) of ABC using a PF-fusion scheme-based database is given 1905 days (or 5.2 years). The obtained percentage error using PF-based multi-sensor fusion is 1.75% (or 98.25% accuracy).

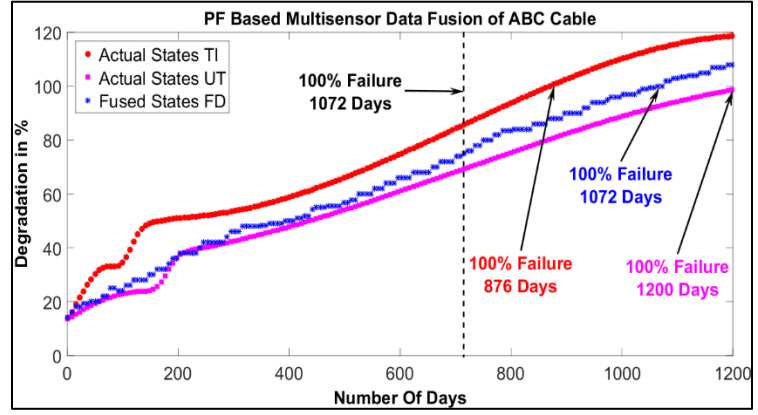


Figure 6: Remaining service life estimation of operational LV ABCs, at SITE-I

The AWGN is inserted into the measurement data as shown in Eq (29). The obtained results indicate that the proposed PF-based multi-sensor fusion scheme works well in the presence of noise. The use of multiple sensor measurement data improves the accuracy and reliability in RUL estimation of live ABCs installed in coastal areas. The percentage error in RUL



estimation of active ABC at Site-I is decreased when the data from multiple measurement modes are used (i.e. fusion of UT and TI-based NDT measurement data).

Figures 7, 8, and 9 display f-step forecasting graphs of damage growth rate in functional ABC cable insulating material, expressed as percentages, set up at Site-I. These plots utilize data from PF-fusion, Ultrasonic listening, and Thermal imaging databases, respectively. Figure 7a demonstrates the one-step estimation plot. The entire process gets started by estimating the second state (i.e., the eighth day) employing the first state's complete information. The PF-based sensor fusion method predicts every single future state one step in advance. The graphical representation of predicted states begins with the second state (8th day), which is the first estimated state after the first state. The latest data generated by the 1-step prediction operation are used as a basis to determine the error margin that occurs between predicted and actual values. Equation (26) generates the particle weight for the subsequent prediction because the technique continuously improves. Equation (28) estimates the one-step prediction scheme's RMSE (via FD data), which is 0.0435.

The next figure 7b depicts the two-step forecasting plot. The procedure entails predicting the second and third states (the eighth and fifteenth days) utilizing the initial day's state and measurement. The algorithm employs a two-step prediction process to forecast each pair of two future states. The graphical representation of predicted states begins with the third state (15th day), that is, the second estimated state compared to the first state. The outcomes achieved serve as a basis for establishing the margin of error. As the algorithm refines its predictions, Equation (27) calculates the weight of particles for the next prediction.

The Root-Mean-Square Error (RMSE) of the 2-step forecasting scheme derived from Equation (28) is 0.3482. Table 5 shows the RMSE scores for 1—to 2-step forecast methods for the fused database of functional ABC cable set up at Site-I. The outcomes show that when measurement data is missing or there is less measurement data (without an update step), prediction results are error-prone. In other words, enhancing the step size of the f-step prediction-based PF technique results in much greater RMSE values.

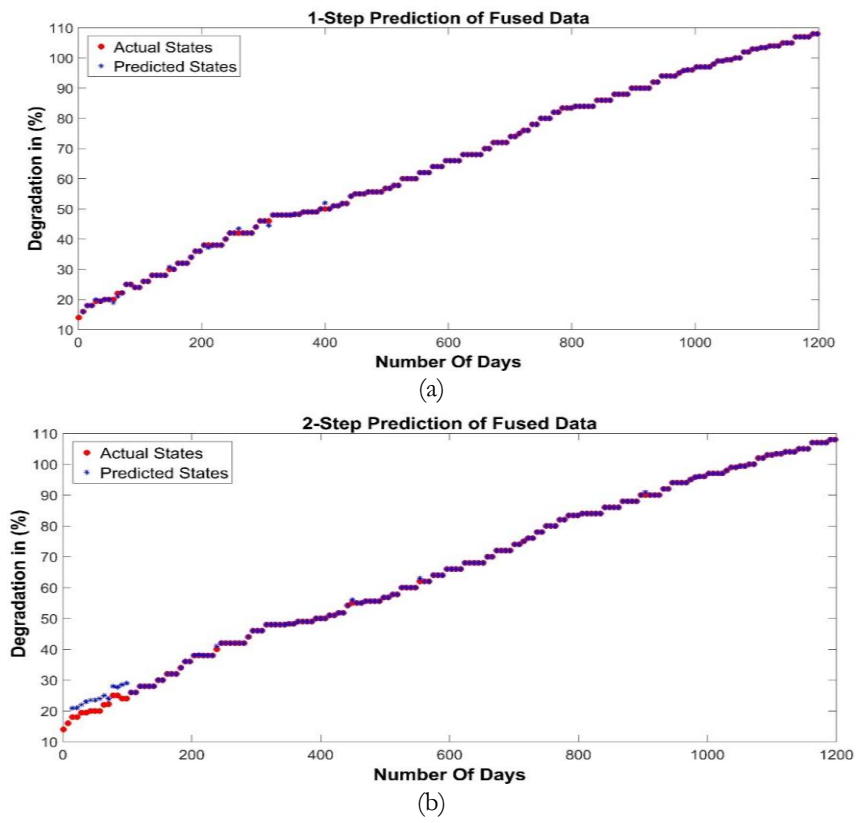




Figure 7: Forecast of damage growth rate in the insulating layer of currently live ABC cable via fused data to number of days, at SITE-I, (a) 1-step prediction. (b) 2-step prediction.

Figures 8(a) and 8(b) demonstrate f-step estimation plots (1-step to 2-step prediction graphs) of deterioration increase in working ABC cables thermal insulation, expressed as percentages, according to genuine SITE-I Ultrasonic listening-based field measurements. The process mirrors the one discussed in Figure. 7. Briefly, figure 8a shows the one-step estimation plot, starting with the second state (eighth day) estimated from the first state's complete data. The PF-based sensor fusion method predicts each future state one step ahead, beginning with the second (eighth day) state. The latest prediction data determines the error margin between predicted and actual values.

Table 5: Root Mean Square Error of Actual and Predicted States of ABCs At Site-I

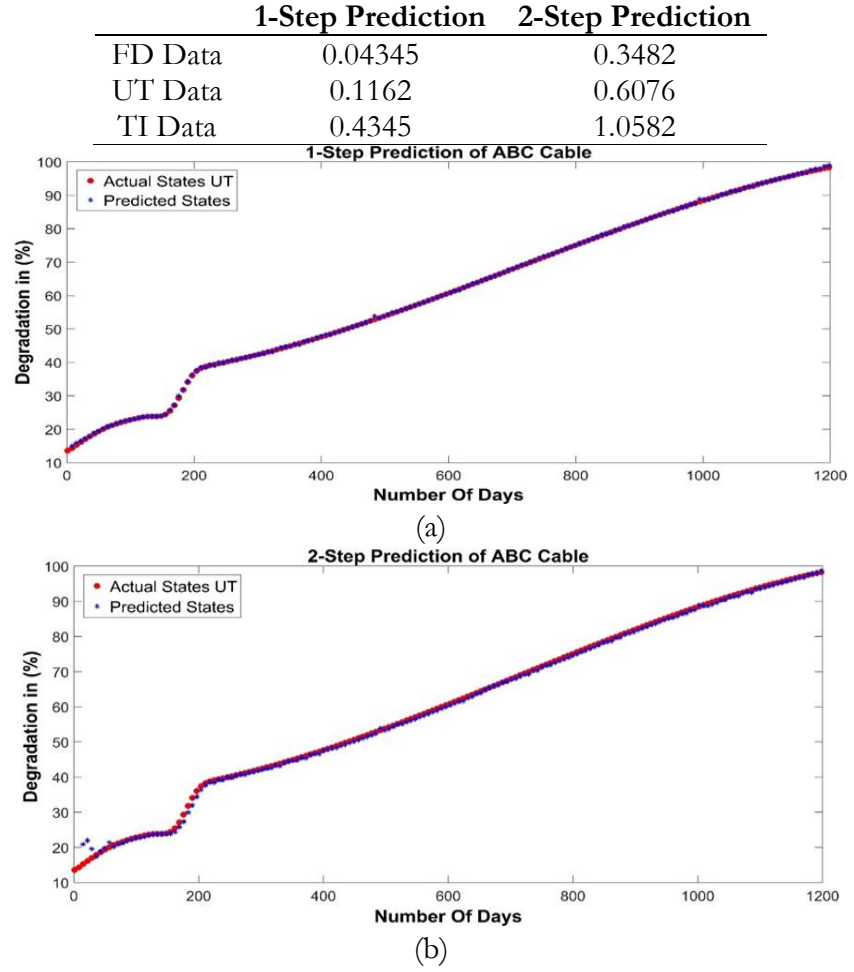


Figure 8: Forecast of damage growth rate in the insulating layer of currently live ABC cable via Ultrasonic listening data in relation to number of days, at SITE-I, (a) 1-step prediction. (b) 2-step prediction.

Figure 8b illustrates the two-step forecasting plot, predicting the second and third states (eighth and fifteenth days) from the initial day's data. The algorithm forecasts each pair of future states, starting with the third state (fifteenth day). The outcomes obtained through the 1- to 2-step estimation techniques are utilized to determine the error margin. The weight of particles in the subsequent estimation is obtained via Equations (26) and (27) for this 1-step and 2-step estimation procedures, respectively. The RMSE values have been calculated (via UT information), for both 1-step to 2-step forecasting methods employing Equation (28) are 0.1162 and 0.6076, respectively, and are listed in Table 5.

Comparably Figures 9(a) and 9(b) show 1- to 2-step forecasting graphs of deterioration increase in ABC cable insulation utilizing thermal image analysis NDT-acquired field measurements. The root-mean-square error values (via TI data) for both 1-step and 2-step estimation methods via Equation (28) are 0.4345 and 1.0582, respectively, as shown in Table 5. This f-step PF-based estimation method works successfully even when the sensor information contains noise (SNR = 10 in this study). The outcomes demonstrate that raising the step size within the f-step prediction-based PF techniques causes more substantial RMSE values. This suggested PF-based f-step prediction setup can be applied to any kind of sealed electrical transmission cable to estimate the damage growth rates.

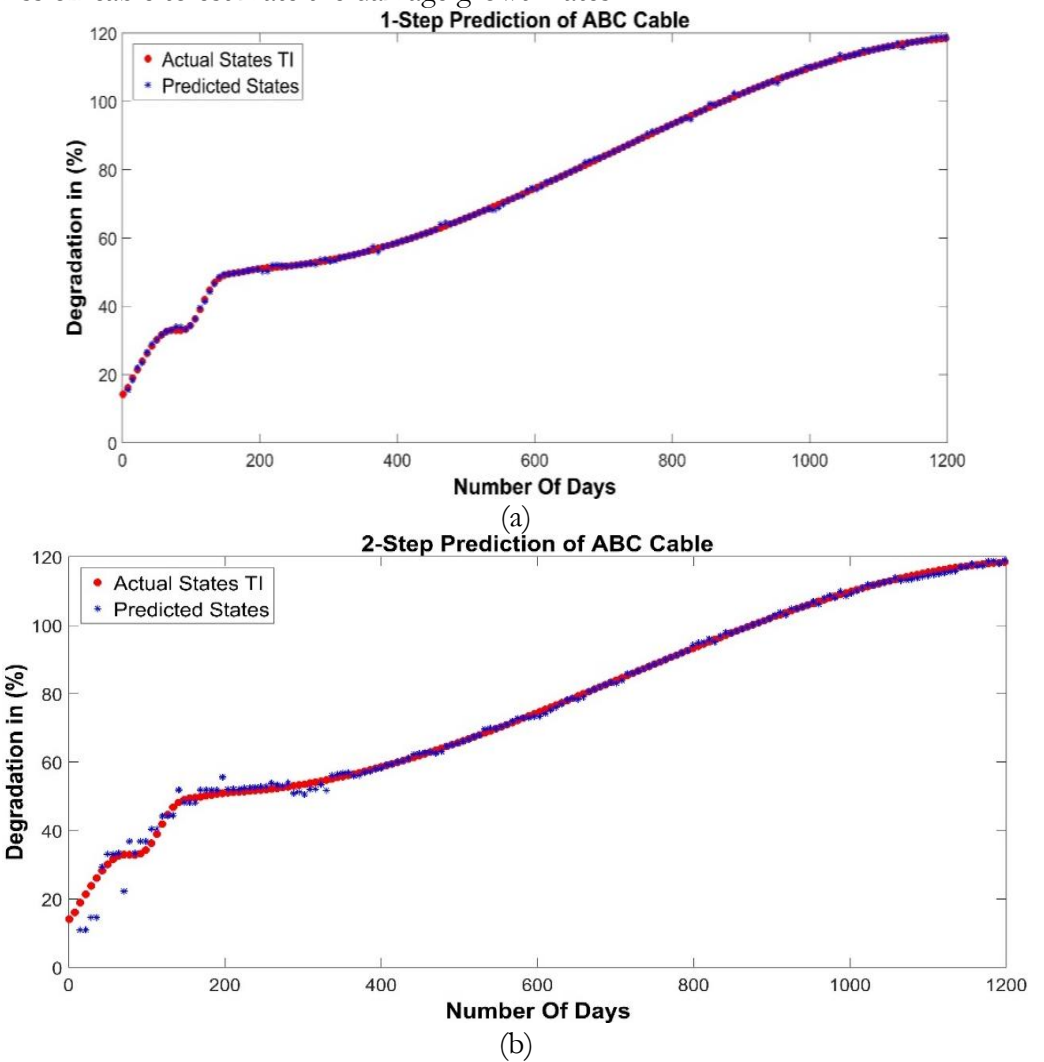


Figure 9: Forecast of damage growth rate in the insulating layer of currently live ABC cable via thermal scanning data to number of days, at SITE-I, (a) 1-step prediction. (b) 2-step prediction.

Conclusion:

A Particle Filter (PF)-based data fusion scheme was proposed for estimating the Remaining Useful Life (RUL) of Live ABC cables installed in coastal areas. Results from multiple databases demonstrate the effectiveness of the proposed RUL estimation scheme. The data fusion technique assumes statistical independence among measurement processes, with Principal Component Analysis (PCA) used to validate this assumption. Results indicate improved accuracy in RUL estimation when data from multiple measurement modes are fused.



Furthermore, an f-step forecasting program incorporated into the PF-based predictive technique has been suggested to forecast subsequent deterioration increases in the thermal insulation of energized overhead electrical cables. The framework changes calculated states via measurements and forecasts future states utilizing the f-step forecasting approach. The scheme is validated using historical measurement data from energized ABC cables acquired in coastal areas, considering noise. The precision of expected outcomes was assessed via Step error evaluation methods in the form of Root-Mean-Square-Error (RMSE). The RMSEs in predicted results for SITE-I ranged from 0.0435 to 0.3482 (Fused data), 0.1162 to 0.6076 (UT data), and 0.4345 to 1.0582 (TI data), respectively.

In addition, the suggested method and setup have been fairly helpful for the occurrence of multiple additional damages in shielded overhead transmission lines that have low tension (LT) and high tension (HT). This versatility underscores the utility of both schemes. The PF-based multi-sensor fusion scheme enhances accuracy and reliability in estimating the RUL of insulated active power cables. Comparably, the PF-based f-step forecasting framework correctly forecasts subsequent deterioration developments in the thermal insulation of ABC cables while in service. As a result, both strategies can be utilized for condition-based predictive servicing of overhead shielded wires.

Acknowledgment: The manuscript has not been published or submitted to other journals previously.

Author's Contribution:

Author 1: Manuscript writing, Software, Methodology, Data curation, original draft, visualization, and conceptualization.

Author 2: Methodology, Writing, Visualization, Conceptualization.

Author 3: Visualization, Resources, Formal Analysis.

Author 4: Visualization, and Formal Analysis.

Conflict of Interest: Authors have no conflict of interest in publishing this manuscript in IJIST. **Project Details.** Not applicable.

References:

- [1] A. Fazal, M. Hao, A. S. Vaughan, G. Chen, J. Cao, and H. Wang, "The effect of composition and processing on electric characteristics of XLPE in HVDC cable applications," 34th Electr. Insul. Conf. EIC 2016, no. June, pp. 440–443, 2016, doi: 10.1109/EIC.2016.7548632.
- [2] M. T. Hagh, "21st International Conference on Electricity Distribution Paper 0452 DESIGN AND INSTALLATION OF FIRST 20 kV SPACER CABLE IN IRAN 21 st International Conference on Electricity Distribution Mechanical design," no. 0452, pp. 6–9, 2011.
- [3] C. Landinger, J. W. Mcauliffe, H. Wire, B. Dagenhart, and W. A. Thue, "SAFETY CONSIDERATIONS OF AERIAL SYSTEMS USING INSULATED AND COVERED WIRE AND CABLE," IEEE Trans. Power Deliv., vol. 12, no. 2, pp. 1012–1016, 1997.
- [4] Z. Zhang, P. D. S. Assala, and L. Wu, "Residual life assessment of 110 kV XLPE cable," Electr. Power Syst. Res., vol. 163, pp. 572–580, 2018, doi: 10.1016/j.epsr.2017.12.027.
- [5] M. T. Hagh, "DESIGN AND INSTALLATION OF FIRST 20 kV SPACER CABLE IN IRAN," no. 0452, pp. 6–9, 2011.
- [6] V. T. Morgan, "The Thermal Conductivity of Crosslinked Polyethylene Insulation in Aerial Bundled Cables," IEEE Trans. Electr. Insul., vol. 26, no. 6, pp. 1153–1158, 1991, doi: 10.1109/14.108153.
- [7] D. Danley, "Technical standards for PV/storage/generator microgrids," GHTC 2017 IEEE Glob. Humanit. Technol. Conf. Proc., vol. 2017-Janua, pp. 1–6, 2017, doi: 10.1109/GHTC.2017.8239303.

- [8] M. Omidiora and M. Lehtonen, "Mitigation of lightning flashover from tree to medium voltage aerial cable using shield wire," IEEE Trans. Power Deliv., vol. 32, no. 4, pp. 1924–1934, 2017, doi: 10.1109/TPWRD.2016.2585104.
- [9] W. Choo, G. Chen, and S. G. Swingler, "Electric field in polymeric cable due to space charge accumulation under DC and temperature gradient," IEEE Trans. Dielectr. Electr. Insul., vol. 18, no. 2, pp. 596–606, 2011, doi: 10.1109/TDEI.2011.5739466.
- [10] G. C. Montanari, G. Mazzanti, and L. Simoni, "Progress in electrothermal life modeling of electrical insulation during the last decades," IEEE Trans. Dielectr. Electr. Insul., vol. 9, no. 5, pp. 730–745, 2002, doi: 10.1109/TDEI.2002.1038660.
- [11] L. Boukezzi, S. Rondot, O. Jbara, and A. Boubakeur, "Study of thermal aging effects on the conduction and trapping of charges in XLPE cable insulations under electron beam irradiation," Radiat. Phys. Chem., vol. 149, pp. 110–117, 2018, doi: 10.1016/j.radphyschem.2018.04.006.
- [12] Y. Bicen, "Trend adjusted lifetime monitoring of underground power cable," Electr. Power Syst. Res., vol. 143, pp. 189–196, 2017, doi: 10.1016/j.epsr.2016.10.045.
- [13] M. A. Shahid, T. M. Khan, T. Zafar, M. F. Hashmi, and M. Imran, "Health diagnosis scheme for in-service low voltage Aerial Bundled Cables using super-heterodyned airborne Ultrasonic testing," Electr. Power Syst. Res., vol. 180, no. November 2019, p. 106162, 2020, doi: 10.1016/j.epsr.2019.106162.
- [14] T. Zafar, T. Khan, A. Alam, W. Bin Yousuf, M. A. Shahid, and F. Hashmi, "Prognosis study of live aerial bundled cables in coastal areas using historical super-heterodyne ultrasonic listening data," Electr. Power Syst. Res., vol. 189, no. June, p. 106591, 2020, doi: 10.1016/j.epsr.2020.106591.
- [15] M. Hassan, Khan, T. M., Abbas, S., Shahid, M. A., Tariq, S. T., and F. Amir, "Hassan, M., Khan, T. M., Abbas, S., Shahid, M. A., Tariq, S. T., Amir, F. (2020). 'Degradation assessment of in-service Aerial Bundled Cables in coastal areas leading to Prognosis using Infrared Thermography'. Manuscript submitted for publication.".
- [16] Z. Xu et al., "Application of temperature field modeling in monitoring of optic-electric composite submarine cable with insulation degradation," Meas. J. Int. Meas. Confed., vol. 133, pp. 479–494, 2019, doi: 10.1016/j.measurement.2018.10.028.
- [17] L. Boukezzi, L. Bessissa, A. Boubakeur, and D. Mahi, "Neural networks and fuzzy logic approaches to predict mechanical properties of XLPE insulation cables under thermal aging," Neural Comput. Appl., vol. 28, no. 11, pp. 3557–3570, 2017, doi: 10.1007/s00521-016-2259-y.
- [18] A. Levet, J. Colombani, and L. Duponchel, "Studying radiolytic ageing of nuclear power plant electric cables with FTIR spectroscopy," Talanta, vol. 172, no. March, pp. 139–146, 2017, doi: 10.1016/j.talanta.2017.05.046.
- [19] Y. Kemari, A. Mekhaldi, and M. Teguar, "Experimental investigation and signal processing techniques for degradation assessment of XLPE and PVC/B materials under thermal aging," IEEE Trans. Dielectr. Electr. Insul., vol. 24, no. 4, pp. 2559–2569, 2017, doi: 10.1109/TDEI.2017.006399.
- [20] P. R. Muniz, J. L. Teixeira, N. Q. Santos, P. L. Q. Magioni, S. P. N. Cani, and J. F. Fardin, "Prospects of life estimation of low voltage electrical cables insulated by PVC by emissivity measurement," IEEE Trans. Dielectr. Electr. Insul., vol. 24, no. 6, pp. 3951–3958, 2017, doi: 10.1109/TDEI.2017.006868.
- [21] T. Khan, P. Ramuhalli, and S. C. Dass, "Particle-filter-based multisensor fusion for solving low-frequency electromagnetic NDE inverse problems," IEEE Transactions on Instrumentation and Measurement, vol. 60, no. 6. pp. 2142–2153, 2011. doi: 10.1109/TIM.2011.2117170.
- [22] J. Dion, M. Kumar, and P. Ramuhalli, "Multi-sensor data fusion for high-resolution



- material characterization," AIP Conf. Proc., vol. 894, no. March, pp. 1189–1196, 2007, doi: 10.1063/1.2718101.
- [23] G. Simone and F. C. Morabito, "NDT image fusion using eddy current and ultrasonic data," COMPEL The International Journal for Computation and Mathematics in Electrical and Electronic Engineering, vol. 20, no. 3. pp. 857–868, 2001. doi: 10.1108/03321640110394030.
- [24] Z. Liu, D. S. Forsyth, J. P. Komorowski, K. Hanasaki, and T. Kirubarajan, "Survey: State of the art in NDE data fusion techniques," IEEE Transactions on Instrumentation and Measurement, vol. 56, no. 6. pp. 2435–2451, 2007. doi: 10.1109/TIM.2007.908139.
- [25] L. Li, K. Tsukada, K. Hanasaki, and Z. Liu, "Fusion of multi-frequency eddy current signals-by using wavelet analysis method," Proc. 5th Int. Conf. Inf. Fusion, FUSION 2002, vol. 1, no. February 2002, pp. 108–113, 2002, doi: 10.1109/ICIF.2002.1021138.
- [26] X. E. Gros, Z. Liu, K. Tsukada, and K. Hanasaki, "Experimenting with pixel-level NDT data fusion techniques," IEEE Trans. Instrum. Meas., vol. 49, no. 5, pp. 1083–1090, 2000, doi: 10.1109/19.872934.
- [27] T. Zafar, T. Mairaj, A. Alam, and H. Rasheed, "Hybrid resampling scheme for particle filter- based inversion," IET Sci. Meas. Technol., vol. PP, no. 99, pp. 1–11, 2020, doi: 10.1049/iet-smt.2018.5531.
- [28] M. S. Arulampalam, S. Maskell, N. Gordon, and T. Clapp, "A Tutorial on Particle Filters for Online Nonlinear / Non-Gaussian Bayesian Tracking," IEEE Trans. Signal Process., vol. 50, no. 2, pp. 174–188, 2002.
- [29] T. Khan and P. Ramuhalli, "A recursive bayesian estimation method for solving electromagnetic nondestructive evaluation inverse problems," IEEE Transactions on Magnetics, vol. 44, no. 7. pp. 1845–1855, 2008. doi: 10.1109/TMAG.2008.921842.
- [30] B. Ristic, A. Sanjeev, and G. Neil, Beyond the Kalman Filter: Particle Filters for Tracking Application, Illustrate., no. 5. Boston: Artech House Publishers, 2004. doi: 10.1007/s13398-014-0173-7.2.
- [31] T. Khan and P. Ramuhalli, "Sequential monte carlo methods for electromagnetic NDE inverse problems-evaluation and comparison of measurement models," IEEE Trans. Magn., vol. 45, no. 3, pp. 1566–1569, 2009, doi: 10.1109/TMAG.2009.2012744.
- [32] Z. Chen and Z. Chen, "Bayesian filtering: from Kalman filters to particle filters, and beyond," Statistics (Ber)., vol. 182, no. 1, 2003, doi: 10.1080/02331880309257.
- [33] M. A. Shahid, T. M. Khan, T. Zafar, F. Hashmi, and F. Amir, "Novel Health Diagnostics schemes analyzing corona discharge of operational Aerial Bundled Cables in coastal regions," IEEE Trans. Power Deliv., vol. 8977, no. c, pp. 1–1, 2020, doi: 10.1109/tpwrd.2020.2974751.
- [34] R. Valles-Novo, J. De Jesus Rangel-Magdaleno, J. M. Ramirez-Cortes, H. Peregrina-Barreto, and R. Morales-Caporal, "Empirical mode decomposition analysis for broken-bar detection on squirrel cage induction motors," IEEE Trans. Instrum. Meas., vol. 64, no. 5, pp. 1118–1128, 2015, doi: 10.1109/TIM.2014.2373513.
- [35] M. Park, D. Kim, and H. S. Oh, "Quantile-Based Empirical Mode Decomposition: An Efficient Way to Decompose Noisy Signals," IEEE Trans. Instrum. Meas., vol. 64, no. 7, pp. 1802–1813, 2015, doi: 10.1109/TIM.2014.2381355.
- [36] I. Ullah et al., "Predictive maintenance of power substation equipment by infrared thermography using a machine-learning approach," Energies, vol. 10, no. 12, 2017, doi: 10.3390/en10121987.
- [37] M. A. Mendes, L. G. R. Tonini, P. R. Muniz, and C. B. Donadel, "Thermographic analysis of parallelly cables: A method to avoid misdiagnosis," Appl. Therm. Eng., vol. 104, pp. 231–236, 2016, doi: 10.1016/j.applthermaleng.2016.05.072.
- [38] M. S. Jadin and S. Taib, "Recent progress in diagnosing the reliability of electrical



- equipment by using infrared thermography," Infrared Phys. Technol., vol. 55, no. 4, pp. 236–245, 2012, doi: 10.1016/j.infrared.2012.03.002.
- [39] Z. A. Jaffery and A. K. Dubey, "Design of early fault detection technique for electrical assets using infrared thermograms," Int. J. Electr. Power Energy Syst., vol. 63, pp. 753–759, 2014, doi: 10.1016/j.ijepes.2014.06.049.
- [40] A. Duarte et al., "Segmentation Algorithms for Thermal Images," Procedia Technol., vol. 16, pp. 1560–1569, 2014, doi: 10.1016/j.protcy.2014.10.178.
- [41] N. Zhu, G. Wang, G. Yang, and W. Dai, "A fast 2D otsu thresholding algorithm based on improved histogram," Proc. 2009 Chinese Conf. Pattern Recognition, CCPR 2009, 1st CJK Jt. Work. Pattern Recognition, CJKPR, pp. 319–323, 2009, doi: 10.1109/CCPR.2009.5344078.
- [42] G. E. Sujji, Y. V. S. Lakshmi, and G. W. Jiji, "MRI Brain Image Segmentation based on Thresholding," Int. J. Adv. Comput. Res., vol. 3, no. 8, pp. 1–5, 2013.
- [43] A. Attig and P. Perner, "The Problem of Normalization and a Normalized Similarity Measure by Online Data," Trans. Case-Based Reason., vol. 4, no. 1, pp. 3–17, 2011.
- [44] T. Khan, L. Udpa, and S. Udpa, "Particle filter based prognosis study for predicting remaining useful life of steam generator tubing," 2011 IEEE Int. Conf. Progn. Heal. Manag. PHM 2011 Conf. Proc., 2011, doi: 10.1109/ICPHM.2011.6024323.
- [45] A. K. Dey and D. Kundu, "Discriminating among the log-normal, weibull, and generalized exponential distributions," IEEE Trans. Reliab., vol. 58, no. 3, pp. 416–424, 2009, doi: 10.1109/TR.2009.2019494.
- [46] W. Bin Yousuf, T. Khan, and T. Ali, "Prognostic Algorithms for Flaw Growth Prediction in an Aircraft Wing," IEEE Transactions on Reliability, vol. 66, no. 2. pp. 478–486, 2017. doi: 10.1109/TR.2017.2676722.
- [47] M. ul Hassan, F. Danish, W. Bin Yousuf, and T. M. R. Khan, "Comparison of different life distribution schemes for prediction of crack propagation in an aircraft wing," Eng. Fail. Anal., vol. 96, no. November 2017, pp. 241–254, 2019, doi: 10.1016/j.engfailanal.2018.10.010.
- [48] H. Abdi and L. J. Williams, "Principal component analysis," Wiley Interdiscip. Rev. Comput. Stat., vol. 2, no. 4, pp. 433–459, 2010, doi: 10.1002/wics.101.
- [49] A. Tefas and I. Pitas, "Principal component analysis," Chemom. Intell. Lab. Syst., vol. 2, pp. 37–52, 1987, doi: 10.2307/1270093.
- [50] J. M. Corchado, S. Sun, G. Villarrubia, T. Li, and J. Bajo, "Resampling methods for particle filtering: identical distribution, a new method, and comparable study," Frontiers of Information Technology & Electronic Engineering, vol. 16, no. 11. pp. 969–984, 2015. doi: 10.1631/fitee.1500199.
- [51] M. Yan et al., Iterative algorithms for electromagnetic NDE signal inversion. Amsterdam, The Netherlands: IOS Press, 1998.



Copyright © by authors and 50Sea. This work is licensed under Creative Commons Attribution 4.0 International License.